

MIMO Communications over Multi-Mode Optical Fibers: Capacity Analysis and Input-Output Coupling Schemes

Peter Kairouz and Andrew Singer

Coordinated Science Laboratory / Department of Electrical and Computer Engineering

University of Illinois at Urbana Champaign, Urbana, Illinois, 61801

Email: {kairouz2, acsinger}@illinois.edu

Abstract

We consider multi-input multi-output (MIMO) communications over multi-mode fibers (MMFs). Current MMF standards, such as OM3 and OM4, use fibers with core radii of $50\ \mu\text{m}$, allowing hundreds of modes to propagate. Unfortunately, due to physical and computational complexity limitations, we cannot couple and detect hundreds of data streams into and out of the fiber. In order to circumvent this issue, two solutions were presented in the literature. The first is to design new fibers with smaller radii so that they can support a desired number of modes. The second is to design multi-core fibers with a reasonable number of cores. However, both approaches are expensive as they necessitate the replacement of currently installed fibers. Moreover, both approaches have limited future scalability. In our work, we present input-output coupling schemes that allow the user to couple and extract a reasonable number of signals from a fiber with many modes (such as those used in OM3 and OM4 standards). This approach is particularly attractive as it is scalable; i.e., the fibers do not have to be replaced every time the number of transmitters or receivers is increased, a phenomenon that is likely to happen in the near future. In addition, fibers with large radii can support higher peak powers relative to fibers with small radii while still operating in the linear regime. However, the only concern is that fibers with more modes suffer from increased mode-dependent losses (MDLs). Our work addresses this last concern.

We present a statistical channel model that incorporates intermodal dispersion, chromatic dispersion, mode dependent losses, and mode coupling. We show that the statistics of the fiber's frequency response are independent of frequency. This simplifies the computation of the average Shannon capacity of the fiber. We later extend this model to include input and output couplers and provide an input-output coupling strategy that leads to an increase in the overall capacity. This strategy can be used whenever channel state information (CSI) is available at the transmitter and the designer has full control over the couplers. We show that the capacity of an $N_t \times N_t$ MIMO system over a fiber with $M \gg N_t$ modes can approach the capacity of an N_t -mode fiber with no mode-dependent losses. Moreover, we present a statistical input-output coupling model in order to quantify the loss in capacity when CSI is not available at the transmitter or there is no control over the input-output coupler. It turns out that the loss, relative to N_t -mode fibers, is minimal (less than 0.5 dB) for a wide range of signal-to-noise ratios (SNRs) and a reasonable range of MDLs. This means that there is no real need to replace the already installed fibers and that our strategy is an attractive

approach to solving the above problem.

I. INTRODUCTION

Since Shannon defined the notion of channel capacity as the fundamental limit on achievable transmission rates with vanishing probability of error, system designers have attempted to reach this limit by leveraging device technology advances and increasingly sophisticated algorithms and architectures. Moore's law, together with advances in signal processing, information theory, and coding theory have enabled us to essentially achieve this fundamental limit for a number of narrow-band wired and wireless communication links. Because of their superior bandwidth-distance product, optical fibers have become extremely popular and have largely replaced traditional copper wire technologies. Optical communication links can support serial data rates that are typically several orders of magnitude higher than their wired or wireless electrical counterparts, such as voice-band or cable modem technology or even high-speed chip-to-chip serial links. Despite their superiority, optical links have limited capacity and the circuits, signal processing, and information theory communities need to completely re-think the design and analysis of optical communication systems in order to address the ever increasing demand for Internet bandwidth. Multi-input multi-output (MIMO) communications over multi-mode fibers (MMFs) holds the promise of improving bandwidth efficiency. However, the capacity of MIMO optical links has not been fully investigated due to the lack of accurate and mathematically tractable channel models. In this paper, we present a detailed linear model for the MIMO multi-mode optical channel and analyze its capacity as a function of input-output coupling as well as other physical parameters. We also introduce an input-output coupling strategy and compare it to the uncontrolled coupling case in terms of achievable rate.

A. Motivation

In an information-intensive era, the demand for Internet bandwidth is increasing at a rate of 56% per year, while the increase in supply is falling behind at a rate of 25% per year [1]. The increase in demand is fueled by the boom in web-based data services such as cloud computing and real-time multimedia applications. As a result, optical fiber communication researchers are looking into new ways of boosting the transmission rate of optical links. Given that polarization division multiplexing (PDM) and wavelength division multiplexing (WDM) have already been exploited [2], the only remaining degree of freedom is space division multiplexing [3]. MIMO optical communication increases the transmission rates of MMF systems by multiplexing a number of independent data streams on different spatial modes. Note that, unlike WDM systems, all the laser sources in this case have the same wavelength. MMF is a dominant type of fiber used for high speed data communication in short-range links such as local area networks (LAN) and data centers [4]. It is usually favored over single-mode fibers because of its relaxed connector alignment tolerances and its reduced transceiver connector costs. Plastic optical fibers are great examples of MMFs with remarkably low installation and operation costs [5]. However, they suffer from mode-dependent losses, mode coupling, intermodal dispersion, and chromatic dispersion (group velocity dispersion) [6]. All these

phenomena will be explained in detail in Section II-A. These limitations make the design and analysis of MIMO multi-mode systems challenging yet exciting.

B. Literature Review

Following the work of Shannon [7], many information theorists investigated the capacity of different channels, including single-input single-output (SISO) channels with memory, channels with constrained input alphabet, and multiple-input multiple-output (MIMO) channels. In their seminal works, Telatar and Foschini *et al.*, independently showed that the capacity of a MIMO flat fading wireless channel, under the Raleigh fading model, scales linearly with respect to the minimum number of antennas at the transmitter and receiver [8], [9]. Since then, the wireless communications community has been focused on developing detection and coding schemes for MIMO systems in order to achieve the aforementioned capacity gains. Recent wireless technologies such as WLAN 802.11n and Long Term Evolution Advanced (LTE-A) are examples of MIMO systems deploying up to 8 transmitters and receivers. More importantly, this MIMO technique is not limited to wireless systems.

Loosely speaking, the number of degrees of freedom (DoF) of a channel is an upper limit on the number of independent data streams that can be transmitted through the channel over a period of time. A more rigorous definition of DoF is given in [10] as the minimal dimension of the received signal space. The quadrature and in-phase components of a passband information signal are two familiar and commonly exploited degrees of freedom in wired and wireless communication systems. Frequency, time, code, quadrature, and polarization states are all well explored and already utilized in commercial optical systems. However, the spatial degree of freedom, which is unique to MMFs, has not been exploited yet in commercial products and is still under research. In 2000, H. R. Stuart was the first to notice the similarity between the multipath wireless channel and the MMF optical channel and suggested using the spatial modes to multiplex several independent data streams onto the fiber [11]. Prior to this finding, single-mode fibers were always considered to be superior to MMFs because of their improved bandwidth-distance product (as SMFs do not suffer from intermodal dispersion). However, we will show in Section III that MMFs have advantages over single-mode fibers from an information theoretic capacity perspective. Therefore, MIMO over MMF seems to be a better route to higher data rates. In fact, Stuart was the first to demonstrate the feasibility of a 2×2 MMF system and to show that there are indeed some capacity gains to be leveraged [11]. However, Stuart's analysis and experiments assumed a radio frequency sub-carrier (~ 1 GHz) instead of an optical carrier (~ 100 THz). This assumption was later relaxed in the work of Shah *et al.* but their treatment did not account for any intermodal dispersion, chromatic dispersion, or mode coupling [12]. Recently, the information theoretic capacity of coherent MMF systems has been studied in [3], where the authors ignored the frequency selectivity of the channel but incorporated the effects of mode coupling. In [13], Keang-Po *et al.* considered the capacity of a frequency selective MMF channel at a particular frequency. They later studied the impact of frequency diversity on the channel capacity for multi-mode fibers with 10 modes [14]. However, their models did not incorporate the effect of mode-dependent phase shifts or chromatic dispersion.

C. Outline and Contributions

In Section II, we present a MIMO channel propagation model that takes intermodal dispersion, chromatic dispersion, mode-dependent losses, and mode coupling into account. In Section III, we compute the Shannon capacity of an M -mode fiber and demonstrate how mode-dependent losses and mode coupling affect it. In Section IV, we analyze the coupling of a reasonable number of laser sources to a fiber with hundreds of modes. We also propose an input-output coupling model and present a coupling strategy: using the input-output couplers to perform a particular type of beamforming. This strategy allows the effective transmission of data along the least lossy subset of end-to-end eigenmodes. The resultant capacity is almost equal to that of a fiber with N_t modes and no modal losses, an ideal case which maximizes the capacity of an $N_t \times N_t$ MIMO system. This coupling strategy can only be used when channel state information (CSI) is available at the transmitter and there is full control over the input-output couplers. In the absence of these conditions, an appropriate random input-output coupling model is used in order to better model the behavior of the system and quantify the expected loss in the fiber's capacity. It turns out that the loss, relative to N_t -mode fibers, is minimal (less than 0.5 dB) for a wide range of SNRs and a reasonable range of MDLs.

D. Random Unitary Matrices

In this section, we provide a brief overview on random unitary matrices and discuss the isotropic invariance property that will prove useful when we compute the capacity of the fiber in Section III. We define $\mathbb{U}(M) := \{\mathbf{U} \in \mathbb{C}^{M \times M} | \mathbf{U}^* \mathbf{U} = \mathbf{U} \mathbf{U}^* = \mathbf{I}_M\}$ to be the space of $M \times M$ unitary matrices. If the distribution of an $M \times N$ random matrix is invariant to left (right) multiplication by any $M \times M$ ($N \times N$) deterministic unitary matrix, it is called left (right) rotationally invariant. Assume the probability distribution function (pdf) $f(\mathbf{A})$ of an $M \times N$ random matrix \mathbf{A} exists, \mathbf{A} is left rotationally invariant if

$$f_{\mathbf{U}\mathbf{A}}(\mathbf{U}\mathbf{A}) = f(\mathbf{A}) \quad (1)$$

where $\mathbf{U} \in \mathbb{U}(M)$, and \mathbf{A} is right rotationally invariant if

$$f_{\mathbf{A}\mathbf{V}}(\mathbf{A}\mathbf{V}) = f(\mathbf{A}) \quad (2)$$

where $\mathbf{V} \in \mathbb{U}(N)$. A random matrix is isotropically invariant if it is left and right rotationally invariant. It turns out that $\mathbb{U}(M)$ forms a compact topological group, and thus a unique uniform measure (up to a scalar multiplication), called Haar measure, can be defined over $\mathbb{U}(M)$ [15], [16]. Random unitary matrices of size $M \times M$ are random matrices sampled uniformly from $\mathbb{U}(M)$.

Lemma 1.1: The pdf of \mathbf{A} , an $M \times M$ random unitary matrix, is isotropically invariant [16].

This lemma will be helpful in the following section.

II. FUNDAMENTALS AND MODELING

Coherent systems use well calibrated phase controlled laser sources and local oscillators operating well in the terahertz regime (hundreds of THz) to transmit and recover the phase and amplitude of an information-bearing signal. On the other hand, non-coherent systems use simple LEDs and photo detectors to transmit and detect the energy of an information signal. Thus, coherent systems are more complex, more expensive, and harder to build and maintain when compared to non-coherent systems. This is why the majority of currently deployed optical systems are non-coherent while a small percentage of the high end systems are coherent. However, coherent systems are becoming more popular as the optoelectronic devices are becoming more affordable. In fact, the state-of-the-art optical systems use both polarization and quadrature multiplexing to multiply the data rate by a factor of four. For example, OC-768 systems use dual polarizations in addition to quadrature phase-shift keying (QPSK) to multiplex four independent data streams and transmit them all at the same time. The OC-768 network has transmission speeds of 40 Gbit/s. This means that in a system using QPSK and dual polarization, the transmitter operates at a frequency of about 10 GHz. Because coherent systems are becoming more popular and affordable, the capacity analysis we perform in Section III is exclusively applicable to coherent systems.

Electromagnetic waves propagating inside the core of a fiber are characterized by Maxwell's equations. When the core radius is sufficiently small, only one solution to the wave equations is supported and the fiber is said to be a single-mode fiber. In multi-mode fiber systems, the core radius is relatively large and hence there is more than one solution (propagation mode) to the wave equation [6]. Ideally, the field inside the core would propagate in different orthogonal modes that do not interact with one another. However, due to manufacturing non-idealities and index of refraction inhomogeneities, the modes may couple. This phenomenon is called mode coupling and is modeled in Section II-A.

A. Fiber Propagation Model

For coherent optical systems operating in the linear regime, the basic form of the baseband transfer function governing the input-output relationship of the i^{th} mode is given by

$$H_i(x, y, z, \omega) = \tilde{\phi}_i(x, y, \omega) e^{-\frac{\kappa_i z}{2}} e^{-j\beta_i(\omega + \omega_c)z} \quad (3)$$

where ω_c is the laser's center frequency, $\tilde{\phi}_i(x, y, \omega)$ is the transverse function (spatial pattern) of the i^{th} mode, κ_i is the mode-dependent attenuation factor, and $\beta_i(\omega + \omega_c)$ is the i^{th} mode's propagation constant [17]. Expanding the function $\beta_i(\omega)$ around ω_c using its Taylor series expansion, and keeping the first and second order derivative terms, we get

$$H_i(x, y, \omega) \approx \phi_i(x, y) e^{\frac{g_i}{2}} e^{-j\theta_i} e^{-j\omega\tau_i} e^{-j\omega^2\alpha_i} \quad (4)$$

where $\phi_i(x, y) = \tilde{\phi}_i(x, y, L, \omega_c)$, $g_i = -\kappa_i L$, $\theta_i = \beta_i(\omega_c) L$, $\tau_i = \beta'_i(\omega_c) L$, and $\alpha_i = \beta''_i(\omega_c) L$. Observe that z has been suppressed as it has been evaluated at L , the fiber's length. The function $\tilde{\phi}_i(x, y, \omega)$ generally depends on ω but since the signal spectrum (tens of GHz) is narrow around the laser's center frequency (hundreds of THz),

we drop this dependency and evaluate it at ω_c . The model in (4) assumes that the propagation of the mode is completely characterized by a second order linear model where the only phenomena exhibited along the i^{th} mode are

- *mode-dependent loss (MDL)*: $g_i = -\kappa_i L$
- *mode-dependent phase shift (MDPS)*: $\theta_i = \beta_i(\omega_c) L$
- *group delay (GD)*: $\tau_i = \beta'_i(\omega_c) L$
- *group velocity dispersion (GVD)*: $\alpha_i = \beta''_i(\omega_c) L$

The mode-dependent losses (MDLs) are negative quantities describing the attenuation experienced by the modal fields. On the other hand, the mode-dependent phase shifts (MDPSs) represent phase shifts experienced by the modal fields. In general, modal fields propagate at different speeds and thus the group delays (GDs) characterize the arrival times of different modes. Therefore, if we transmit a narrow pulse through the fiber, it would appear as a pulse having a width of $T_d = \max_{i,j}\{|\tau_i - \tau_j|\}$ at the output of the fiber. The quantity T_d is referred to as the channel's delay spread. Assume, without loss of generality, that the group delays are sorted in increasing order, τ_1 being the smallest and τ_M being the largest. In this case, T_d is given by

$$\begin{aligned} T_d &= \max_{i,j}\{|\tau_i - \tau_j|\} \\ &= \tau_M - \tau_1 \\ &= L \left(\beta'_M(\omega_c) - \beta'_1(\omega_c) \right) \end{aligned} \quad (5)$$

Thus, T_d is directly proportional to the length of the fiber. The pulse broadening phenomenon, due to nonzero T_d , is called intermodal dispersion and is a serious performance limitation in MMF systems. The group velocity dispersion (GVD), also called chromatic dispersion (CD), suggests that different frequencies coupled to the same mode propagate at different speeds and hence broadening occurs to the field propagating in a particular mode. This phenomenon is called intra-modal dispersion. In a first-order model, intermodal dispersion is assumed to dominate over intra-modal dispersion and the GVD term is typically neglected, especially for shorter lengths L . Furthermore, since we are not interested in analyzing the field at every point (x, y) in the fiber's core, we suppress this term to obtain the following expression:

$$H_i(\omega) \propto e^{\frac{g_i}{2}} e^{-j\theta_i} e^{-j\omega\tau_i} e^{-j\omega^2\alpha_i} \quad (6)$$

Ideally, the field at the output due to the i^{th} mode is given by $r_i(t) = s_i \star h_i(t)$, where $s_i(t)$ is the field at the input due to the same mode. Thus, the frequency domain vector representation of the modal fields at the output of the fiber is given by

$$\begin{bmatrix} r_1(\omega) \\ \vdots \\ r_M(\omega) \end{bmatrix} = \begin{bmatrix} H_1(\omega) & & \\ & \ddots & \\ & & H_M(\omega) \end{bmatrix} \begin{bmatrix} s_1(\omega) \\ \vdots \\ s_M(\omega) \end{bmatrix} \quad (7)$$

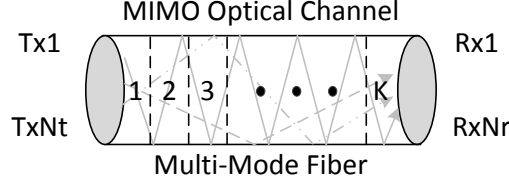


Fig. 1: A multi-mode fiber with K propagation sections

where the off-diagonal entries are zero because the modes are assumed to be orthogonal. This analysis neglects the existing fiber aberrations such as fiber bends, index of refraction inhomogeneities, and random vibrations, and is therefore incomplete. In fact, the modes interact with one another and exchange energy as they propagate along the fiber, complicating the analysis of the wave propagation. The treatment we present was first applied to polarization mode dispersion (PMD) in [18] and was then generalized to model mode coupling in [13]. In the regime of high mode coupling, for example when plastic optical fibers are used, an MMF with M modes¹ is split into $K \gg 1$ statistically independent longitudinal sections as depicted in Figure 1. The number of sections K is equal to L/l_c , where l_c represents the correlation length of the fiber. The frequency response of each section is given by

$$\mathbf{H}^k(\omega) = \mathbf{U}^k \mathbf{\Lambda}^k(\omega) \mathbf{V}^{k*} \quad \text{for } k = 1, \dots, K \quad (8)$$

where \mathbf{U}^k and \mathbf{V}^k are $M \times M$ frequency-independent projection matrices (unitary matrices) describing the modal coupling via a phase and energy shuffling process at the input and output of each section and

$$\mathbf{\Lambda}^k(\omega) = \text{diag} \left(e^{\frac{1}{2} g_1^k - j\theta_1^k - j\omega\tau_1^k - j\omega^2\alpha_1^k}, \dots, e^{\frac{1}{2} g_M^k - j\theta_M^k - j\omega\tau_M^k - j\omega^2\alpha_M^k} \right) \quad (9)$$

is the propagation matrix describing the ideal (uncoupled) field propagation in the k^{th} section. This model assumes that mode coupling occurs at the interface of different sections while the propagation in each section is ideal (and is described by $\mathbf{\Lambda}^k(\omega)$). In (9), the vectors $\mathbf{g}^k = (g_1^k, \dots, g_M^k)$, $\boldsymbol{\theta}^k = (\theta_1^k, \dots, \theta_M^k)$, $\boldsymbol{\tau}^k = (\tau_1^k, \dots, \tau_M^k)$, and $\boldsymbol{\alpha}^k = (\alpha_1^k, \dots, \alpha_M^k)$ represent the uncoupled MDL, MDPS, GD, and GVD coefficients in the k^{th} section. Here, $g_i^k = -\kappa_i^k l_c$, $\theta_i^k = \beta_i^k(\omega_c) l_c$, $\tau_i^k = \beta_i'^k(\omega_c) l_c$, and $\alpha_i^k = \beta_i''^k(\omega_c) l_c$ are not necessarily identical across the M modes and K sections and will be modeled as random variables in Section II-B. The overall channel frequency response is equal to the product of the frequency responses of the K sections and is given by

$$\mathbf{H}(\omega) = \mathbf{H}^{(K)}(\omega) \dots \mathbf{H}^{(1)}(\omega) \quad (10)$$

Alternatively, one could describe the input output relationship in time domain by

$$\mathbf{H}(t) = \mathbf{H}^{(K)} \star \mathbf{H}^{(K-1)} \dots \mathbf{H}^{(2)} \star \mathbf{H}^{(1)}(t) \quad (11)$$

¹In this work, M refers to all the available spatial degrees of freedom including the x and y polarization states.

In (11), the operation $\mathbf{C}(t) = \mathbf{A} \star \mathbf{B}(t)$ represents a matrix convolution operation. Specifically, the $(i, j)^{th}$ entry of $\mathbf{C}(t)$ is given by

$$c_{ij}(t) = \sum_{l=1}^M a_{il} \star b_{lj}(t) \quad (12)$$

where M is the dimension of the square matrices $\mathbf{A}(t)$ and $\mathbf{B}(t)$ and \star denotes the convolution operator.

B. Random Propagation Model

We now develop a random propagation model for the MIMO optical channel. The random model we introduce is an extended variant of what was presented in [13] and [19]. The per-section coupling matrices \mathbf{U}^k and \mathbf{V}^k are modeled as independent and identically distributed (i.i.d.) random unitary matrices with arbitrary distributions. We assume that the propagation characteristics g_i^k , θ_i^k , α_i^k , and τ_i^k are all independent random quantities. In addition, each of \mathbf{g}^k , $\boldsymbol{\theta}^k$, $\boldsymbol{\tau}^k$, and $\boldsymbol{\alpha}^k$ has zero mean identically distributed, but possibly correlated, entries. The zero mean assumption is not restrictive because the mean MDL, MDPS, GD, and GVD do not affect the capacity of the fiber. Even though the propagation characteristics are identically distributed within a particular section, they need not have the same distributions from one section to the other. We define σ_k to be the standard deviation of the uncoupled MDLs in the k^{th} section: $\sigma_k = \sqrt{\text{Var}(g_i^k)} = l_c \sqrt{\text{Var}(\kappa_i^k)}$. At any fixed frequency ω_0 , the overall frequency response in (10) can be written as

$$\mathbf{H}(\omega_0) = \mathbf{U}_H(\omega_0) \boldsymbol{\Lambda}_H(\omega_0) \mathbf{V}_H^*(\omega_0) \quad (13)$$

by the singular value decomposition (SVD) of $\mathbf{H}(\omega_0)$. In (13), all the matrices are random frequency dependent square matrices and

$$\boldsymbol{\Lambda}_H(\omega_0) = \text{diag}\left(e^{\frac{1}{2}\rho_1}, \dots, e^{\frac{1}{2}\rho_M}\right) \quad (14)$$

contains the *end-to-end eigenmodes*, singular values of $\mathbf{H}(\omega_0)$. We note that the end-to-end eigenmodes are not actual solutions to the wave equation, but rather they characterize the effective overall propagation through the fiber. The vector $\boldsymbol{\rho} = (\rho_1, \rho_2, \dots, \rho_M)$ contains the *end-to-end mode-dependent losses*, the logarithms of the eigenvalues of $\mathbf{H}(\omega_0) \mathbf{H}^*(\omega_0)$. These quantities are obviously frequency dependent random variables as they are the logarithms of the eigenvalues of a frequency dependent random matrix. The *accumulated mode-dependent loss variance* is defined as

$$\xi^2 = \sigma_1^2 + \sigma_2^2 + \dots + \sigma_K^2 \quad (15)$$

where ξ is measured in units of the logarithm of power gain and can be converted to decibels by multiplying its value by $10/\ln 10$ [13]. When all sections have identical distributions for the MDLs, Equation (15) reduces to $\xi^2 = K\sigma^2$ because $\sigma_k = \sigma$ for all k .

III. CAPACITY OF MULTI-MODE FIBERS

In this section, we compute the capacity of coherent MMF systems under the presence of mode-dependent phase shifts (MDPSs), mode-dependent losses (MDLs), group delay (GD), chromatic dispersion (CD), and mode coupling. Table I summarizes the parameters governing the random propagation model presented in Section II-B. Each of the

TABLE I: Random propagation model

fiber's frequency response	$\mathbf{H}(\omega) = \mathbf{H}^K(\omega) \dots \mathbf{H}^1(\omega)$
per-section response	$\mathbf{H}^k(\omega) = \mathbf{U}^k \mathbf{\Lambda}^k(\omega) \mathbf{V}^{k*}$
per-section coupling matrices	\mathbf{U}^k and \mathbf{V}^k
uncoupled MDL	$\mathbf{g}^k = (g_1^k, \dots, g_M^k)$
uncoupled MDPS	$\boldsymbol{\theta}^k = (\theta_1^k, \dots, \theta_M^k)$
uncoupled GD	$\boldsymbol{\tau}^k = (\tau_1^k, \dots, \tau_M^k)$
uncoupled GVD	$\boldsymbol{\alpha}^k = (\alpha_1^k, \dots, \alpha_M^k)$
uncoupled MDL variance	$\sigma_k^2 = \text{Var}(g_i^k) = l_c^2 \text{Var}(\kappa_i^k)$
accumulated MDL variance	$\xi^2 = \sigma_1^2 + \sigma_2^2 + \dots + \sigma_K^2$

vectors \mathbf{g}^k , $\boldsymbol{\theta}^k$, $\boldsymbol{\tau}^k$, and $\boldsymbol{\alpha}^k$ has zero mean identically distributed, but possibility correlated, entries. Moreover, the vectors \mathbf{g}^{k_1} , $\boldsymbol{\theta}^{k_1}$, $\boldsymbol{\tau}^{k_1}$, and $\boldsymbol{\alpha}^{k_1}$ are independent of \mathbf{g}^{k_2} , $\boldsymbol{\theta}^{k_2}$, $\boldsymbol{\tau}^{k_2}$, and $\boldsymbol{\alpha}^{k_2}$ for $k_1 \neq k_2$. However, they can have the same statistical distributions. Recall, from Section II-B, that the k^{th} section propagation matrix is given by

$$\begin{aligned} \mathbf{\Lambda}^k(\omega) &= \text{diag} \left(e^{\frac{1}{2}g_1^k - j\theta_1^k - j\omega\tau_1^k - j\omega^2\alpha_1^k}, \dots, e^{\frac{1}{2}g_M^k - j\theta_M^k - j\omega\tau_M^k - j\omega^2\alpha_M^k} \right) \\ &= \boldsymbol{\Theta}^k \mathbf{T}^k \mathbf{A}^k \mathbf{G}^k \end{aligned} \quad (16)$$

where $\boldsymbol{\Theta}^k = \text{diag} \left(e^{-j\theta_1^k}, \dots, e^{-j\theta_M^k} \right)$, $\mathbf{T}^k = \text{diag} \left(e^{-j\omega\tau_1^k}, \dots, e^{-j\omega\tau_M^k} \right)$, $\mathbf{A}^k = \text{diag} \left(e^{-j\omega^2\alpha_1^k}, \dots, e^{-j\omega^2\alpha_M^k} \right)$, and $\mathbf{G}^k = \text{diag} \left(e^{\frac{1}{2}g_1^k}, \dots, e^{\frac{1}{2}g_M^k} \right)$.

A. Frequency Flat Channel Capacity

We first study the capacity of the system when the channel's delay spread and CD are negligible. The more general frequency selective case is handled in Section III-B. In this regime, $\max_{ij} |\tau_i^k - \tau_j^k| \approx 0$ and $\max_i |\alpha_i^k| \approx 0$ and hence $\tau_i^k = \tau^k$ and $\alpha_i^k = 0$ for all i and k . Therefore, the k^{th} section propagation matrix is given by

$$\begin{aligned} \mathbf{\Lambda}^k(\omega) &= \text{diag} \left(e^{\frac{1}{2}g_1^k - j\theta_1^k - j\omega\tau_1^k - j\omega^2\alpha_1^k}, \dots, e^{\frac{1}{2}g_M^k - j\theta_M^k - j\omega\tau_M^k - j\omega^2\alpha_M^k} \right) \\ &= e^{-j\omega\tau^k} \text{diag} \left(e^{\frac{1}{2}g_1^k - j\theta_1^k}, \dots, e^{\frac{1}{2}g_M^k - j\theta_M^k} \right) \\ &= e^{-j\omega\tau^k} \boldsymbol{\Theta}^k \mathbf{G}^k \\ &= e^{-j\omega\tau^k} \mathbf{\Lambda}^k \end{aligned} \quad (17)$$

where $\mathbf{\Lambda}^k = \boldsymbol{\Theta}^k \mathbf{G}^k$. Therefore, the overall response can be written as

$$\begin{aligned} \mathbf{H}(\omega) &= e^{-j\omega \sum_{k=1}^K \tau^k} \mathbf{U}^K \mathbf{\Lambda}^K \mathbf{V}^{K*} \dots \mathbf{U}^1 \mathbf{\Lambda}^1 \mathbf{V}^{1*} \\ &= e^{-j\omega \sum_{k=1}^K \tau^k} \mathbf{U}_H \mathbf{\Lambda}_H \mathbf{V}_H^* \end{aligned} \quad (18)$$

where \mathbf{U}_H , $\mathbf{\Lambda}_H$, and \mathbf{V}_H^* are obtained by applying the singular value decomposition to $\mathbf{U}^K \mathbf{\Lambda}^K \mathbf{V}^{K*} \dots \mathbf{U}^1 \mathbf{\Lambda}^1 \mathbf{V}^{1*}$. Observe that \mathbf{U}_H , $\mathbf{\Lambda}_H$, and \mathbf{V}_H^* are all frequency independent. The term $e^{-j\omega \sum_{k=1}^K \tau^k}$ is a delay term and can be neglected if we assume that the transmitter and receiver are synchronized. Thus, the channel is frequency flat and is given by

$$\mathbf{H} = \mathbf{U}_H \mathbf{\Lambda}_H \mathbf{V}_H^* \quad (19)$$

Consequently, the input-output relationship under this frequency flat channel model in (19) is given by

$$\mathbf{y} = \mathbf{H}\mathbf{x} + \mathbf{v} \quad (20)$$

where \mathbf{x} and \mathbf{y} represent the transmitted and received vectors, respectively, and \mathbf{v} represents the modal noise which is modeled as additive white Gaussian noise (AWGN) with covariance matrix $N_0 \mathbf{I}_M$, N_0 being the noise power density per Hz. This assumes that coherent optical communication is used and that electronic noise is the dominant source of noise. In addition, the fiber non-linearities are neglected under the assumption that the signal's peak to average power ratio (PAPR) and peak power are both low enough. This condition is not restrictive because MMFs have large radii and hence can support more power (relative to single mode fibers) while still operating in the linear region. The input-output model in (20) may seem identical to the wireless MIMO flat fading one. However, the Rayleigh fading i.i.d. model does not hold in our case because \mathbf{H} is a product of K terms, each containing a random diagonal matrix sandwiched between two random unitary matrices. Moreover, the entries of \mathbf{H} are correlated. From [8], the capacity of a single instantiation of the channel in (19), when channel state information (CSI) is not available at the transmitter, is given by

$$\begin{aligned} C(\mathbf{H}) &= \log \det \left(\mathbf{I}_M + \frac{\text{SNR}}{M} \mathbf{H}\mathbf{H}^* \right) \\ &= \sum_{n=1}^M \log \left(1 + \frac{\text{SNR}}{M} \lambda_n^2 \right) \quad \text{b/s/Hz} \end{aligned} \quad (21)$$

where $\text{SNR} = P/N_0W$, P representing the total power divided equally across all modes and W representing the available bandwidth in Hz. The λ_n^2 's are the eigenvalues of $\mathbf{H}\mathbf{H}^*$. If CSI is available at the transmitter, the capacity could be further increased through waterfilling [20], [10]. In this case, the transmitter pre-processes the transmit vector \mathbf{x} by allocating powers using a waterfilling procedure and then multiplies \mathbf{x} by \mathbf{V}_H . On the other side, the receiver multiplies the received vector \mathbf{y} by \mathbf{U}_H^* . This effectively turns the MIMO channel into a set of parallel AWGN channels. In optical communications, the beamforming process assumes that the designer can couple the fields of different sources onto the fiber exactly as determined by \mathbf{V}_H . This procedure, though beneficial, is complicated as it necessitates the design of sophisticated reconfigurable mode-selective spatial filters using coherent spatial light modulators [21], [22].

In the above analysis, we considered the capacity of (20) for a given instantiation of \mathbf{H} . However, since \mathbf{H} is random, the channel capacity $C(\mathbf{H})$ is a random variable. In the fast fading regime, the ergodic capacity, expected value of $C(\mathbf{H})$, is desired as it dictates the fastest rate of transmission [10]. On the other hand, in the slow fading

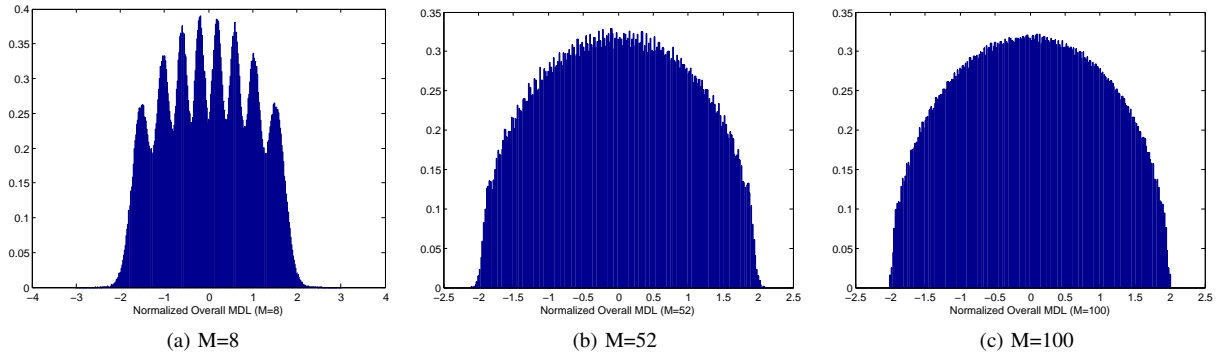


Fig. 2: Distribution of end-to-end MDL

regime, the cumulative distribution function (CDF) of $C(\mathbf{H})$ is desired as it determines the probability of an outage event for a particular rate of transmission [10]. In either case, the cumulative distribution and the expected value of $C(\mathbf{H})$ are both functions of the distribution of $\boldsymbol{\lambda} = (\lambda_1^2, \dots, \lambda_M^2)$, the eigenvalues of $\mathbf{H}\mathbf{H}^*$. From (19), the matrix $\mathbf{H}\mathbf{H}^* = \mathbf{U}_H \boldsymbol{\Lambda}_H^2 \mathbf{U}_H^*$ is Hermitian and its eigenvalues, the squares of the singular values of \mathbf{H} , are real non-negative quantities. Recall from Section II-B that the quantity $\lambda_n = e^{\frac{1}{2}\rho_n}$ refers to the n^{th} end-to-end eigenmode and the quantity ρ_n refers to the n^{th} end-to-end mode dependent loss (MDL). The distribution of the end-to-end MDL values was studied in [13] where it was shown that as M tends to infinity, the ρ_n 's become independent and identically distributed on a semicircle. Their analysis and simulations, however, did not incorporate the effect of mode dependent phase shifts (MDPSs), θ_i^k 's. We now show that the statistical distribution of the end-to-end MDL values is unchanged even when MDPSs are incorporated.

Theorem 3.1: The statistics of \mathbf{H} are independent of mode dependent phase shifts.

Proof: We show that the statistics of $\mathbf{H}^k = \mathbf{U}^k \Theta^k \mathbf{G}^k \mathbf{V}^{k*}$ are the same as those of $\mathbf{H}^k = \mathbf{U}^k \mathbf{G}^k \mathbf{V}^{k*}$ for all $k = 1, \dots, K$. Observe that Θ^k is a unitary matrix that is also random because it has random orthonormal columns. However, Θ^k does not necessarily belong to the class of random unitary matrices as it is not necessarily uniformly distributed over $\mathbb{U}(M)$. Nonetheless, we note that the distribution of $\mathbf{W} = \mathbf{U}^k \Theta^k$ is the same as the distribution of \mathbf{U}^k because

$$\begin{aligned}
 f(\mathbf{W}) &= \int_{\Theta^k} f(\mathbf{W}|\Theta^k) f(\Theta^k) d\Theta^k \\
 &= f(\mathbf{U}^k) \int_{\Theta^k} f(\Theta^k) d\Theta^k \\
 &= f(\mathbf{U}^k)
 \end{aligned} \tag{22}$$

where the second equality holds because for a given instantiation of Θ^k , the random matrix $\mathbf{W}|\Theta^k$ has the same distribution as \mathbf{U}^k (by Lemma 1.1 in Section I-D). Therefore, the statistics of \mathbf{H} are unchanged when the MDPSs are incorporated, and thus the results in [13] carry over to this more general setting. ■

Figure 2 shows that for $M = 100$ the distribution of ρ_n approaches a semicircle. The distributions in Figure 2 were

obtained by generating a large sample of channel matrices \mathbf{H} (for $M = 8$, $M = 52$, and 100) and estimating the distributions of the logarithm of their singular values. Appendix A explains how we can generate random unitary matrices, which are needed to create samples of \mathbf{H} , from matrices with i.i.d. complex Gaussian entries. In this section, we use the following notation

$$\tilde{x} = \frac{x}{\mathbb{E}[x]} \quad (23)$$

where \tilde{x} denotes the energy-normalized version of the random variable x . The average capacity of $C(\mathbf{H})$ is given by

$$C_{\text{avg}} = \sum_{n=1}^M \mathbb{E} \left[\log \left(1 + \frac{\text{SNR}}{M} \tilde{\lambda}_n^2 \right) \right] \quad \text{b/s/Hz} \quad (24)$$

where the average is taken over the statistics of the end-to-end MDL values [10]. Figure 3a shows the average capacity of MMFs for various values of M and $\xi = 4$ dB. The capacity of the system increases with an increasing number of modes. This is intuitive because as the number of modes increases, the fiber's spatial degrees of freedom are increased. Figure 3b shows the effect of accumulated MDLs on the average capacity. An increasing value of ξ results in a capacity equivalent to that of a fiber with fewer modes. This means that as ξ^2 , the accumulated mode-dependent loss variance, increases the system loses its spatial degrees of freedom.

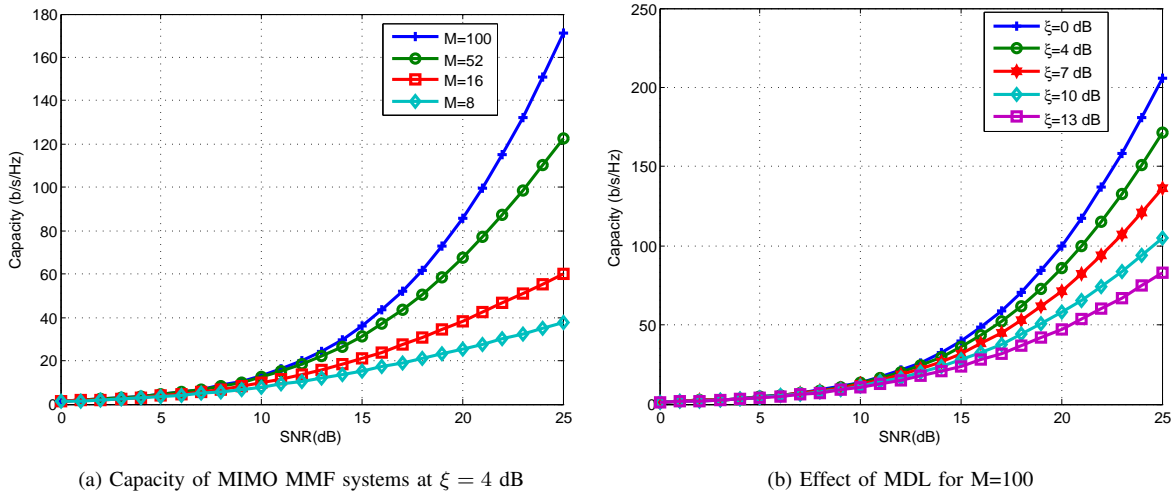


Fig. 3: Ergodic Capacity Analysis

B. Frequency Selective Channel Capacity

When chromatic and intermodal dispersion are taken into account, the fiber's frequency response $\mathbf{H}(\omega)$ becomes frequency selective. Under the same linear assumptions as in the previous section, the input-output relationship is given by

$$\mathbf{y}(t) = \mathbf{H}(t) \star \mathbf{x}(t) + \mathbf{v}(t) \quad (25)$$

where $\mathbf{v}(t)$ is a vector Gaussian process, $\mathbf{x}(t)$ is the input, and $\mathbf{y}(t)$ is the received signal. Recall, from Section II-A, that $\mathbf{H}(\omega_0)$ can be written as

$$\mathbf{H}(\omega_0) = \mathbf{U}_H(\omega_0) \mathbf{\Lambda}_H(\omega_0) \mathbf{V}_H^*(\omega_0) \quad (26)$$

where $\mathbf{U}_H(\omega_0)$, $\mathbf{\Lambda}_H(\omega_0)$, and $\mathbf{V}_H^*(\omega_0)$ all depend on ω_0 . From [10], the capacity of a single instantiation of $\mathbf{H}(\omega)$, when CSI is not available at the transmitter, is equal to

$$C = \frac{1}{2\pi W} \int_0^{2\pi W} \log \det \left(\mathbf{I}_{N_r} + \frac{\text{SNR}}{M} \mathbf{H}(\omega) \mathbf{H}^*(\omega) \right) d\omega \quad \text{b/s/Hz} \quad (27)$$

where W is the bandwidth of the system in Hz and $\text{SNR} = P/N_0W$ [10]. This capacity can be achieved by Orthogonal Frequency Division Multiplexing (OFDM) with N sub-carriers (as N tends to infinity). MIMO OFDM modulation is a popular modulation scheme in wireless communications and is currently being developed for the next generation optical systems [23]. The maximum achievable capacity of a MIMO-OFDM system with N sub-carriers is

$$\begin{aligned} C &= \frac{1}{N} \sum_{i=1}^N \log \det \left(\mathbf{I}_{N_r} + \frac{\text{SNR}}{M} \mathbf{H}_i \mathbf{H}_i^* \right) \\ &= \frac{1}{N} \sum_{i=1}^N \sum_{n=1}^M \log \left(1 + \frac{\text{SNR}}{M} \lambda_{n,i}^2 \right) \quad \text{b/s/Hz} \end{aligned} \quad (28)$$

where $\mathbf{H}_i = \mathbf{H}(\omega_i)$ and $\lambda_{n,i}^2$ is the n^{th} eigenvalue of $\mathbf{H}_i \mathbf{H}_i^*$. When CSI is available at the transmitter, waterfilling can be performed to allocate optimal powers across sub-carriers and transmitters.

In the above analysis, we considered the capacity of (25) for a given instantiation of $\mathbf{H}(\omega)$. In our work, we focus on analyzing the expected capacity of the frequency selective system which is given by

$$C_{\text{avg}} = \mathbb{E} \left[\frac{1}{N} \sum_{i=1}^N \sum_{n=1}^M \log \left(1 + \frac{\text{SNR}}{M} \tilde{\lambda}_{n,i}^2 \right) \right] \quad \text{b/s/Hz} \quad (29)$$

To begin with, if we assume that, in each section, all modes experience the same random loss (i.e., the entries of \mathbf{g}^k are perfectly correlated), then $\mathbf{G}^k = e^{\frac{1}{2}g^k} \mathbf{I}_M$. Furthermore, assume that the K sections are statistically identical. Therefore, $\sigma_k = \sigma$ for all k and $\xi^2 = K\sigma^2$. In this case, the overall response is given by

$$\begin{aligned} \mathbf{H}(\omega) &= \mathbf{H}^K(\omega) \dots \mathbf{H}^1(\omega) \\ &= \mathbf{U}^K \mathbf{\Lambda}^K(\omega) \mathbf{V}^{K*} \dots \mathbf{U}^1 \mathbf{\Lambda}^1(\omega) \mathbf{V}^{1*} \\ &= e^{\frac{1}{2} \sum_{k=1}^K g^k} \mathbf{U}^K \mathbf{\Theta}^K \mathbf{T}^K \mathbf{A}^K \mathbf{V}^{K*} \dots \mathbf{U}^1 \mathbf{\Theta}^1 \mathbf{T}^1 \mathbf{A}^1 \mathbf{V}^{1*} \end{aligned} \quad (30)$$

Observe that, even though $\mathbf{H}(\omega)$ is a function of ω , $\mathbf{H}(\omega) \mathbf{H}(\omega)^* = e^{\sum_{k=1}^K g^k} \mathbf{I}_M$ is independent of ω . This means that $\lambda_{n,i}^2 = \lambda = e^{\sum_{k=1}^K g^k}$ is independent of the frequency index i and the mode number n . Thus, the average capacity of the fiber is given by

$$C_{\text{avg}} = M \mathbb{E} \left[\log \left(1 + \frac{\text{SNR}}{M} \tilde{\lambda}^2 \right) \right] \quad (31)$$

where the average is taken over the statistics of $\tilde{\lambda}^2$. Observe that the average capacity scales linearly with M , the number of modes, and thus the fiber has M degrees of freedom. Therefore, neither group delay nor chromatic dispersion affect the average capacity of the fiber.

We now derive the capacity for the general case (i.e., when the entries of \mathbf{g}^k are potentially independent). The following theorem shows that the statistics of $\mathbf{H}(\omega)$ are independent of ω .

Theorem 3.2: The statistics of $\mathbf{H}(\omega)$ are independent of ω .

Proof: Using the same technique as in the proof of Theorem 3.1, we can show that the statistics of $\mathbf{H}^k(\omega) = \mathbf{U}^k \Theta^k \mathbf{T}^k \mathbf{A}^k \mathbf{G}^k \mathbf{V}^{k*}$ are the same as the statistics of $\mathbf{H}^k = \mathbf{U}^k \mathbf{G}^k \mathbf{V}^{k*}$ by showing that the distribution of $\mathbf{W}^k = \mathbf{U}^k \Theta^k \mathbf{T}^k \mathbf{A}^k$ is equal to the distribution of \mathbf{U}^k . Thus, the statistics of $\mathbf{H}^k(\omega)$ are independent of ω . ■

This result shows that the statistics of the eigenvalues of $\mathbf{H}_i \mathbf{H}_i^*$ are identical for all i . Therefore, the average capacity expression can now be rewritten as

$$C_{\text{avg}} = \sum_{n=1}^M \mathbb{E} \left[\log \left(1 + \frac{\text{SNR}}{M} \tilde{\lambda}_n^2 \right) \right] \quad \text{b/s/Hz} \quad (32)$$

which is identical to the average capacity of frequency flat optical MIMO systems. Therefore, the results of the previous section carry over to the frequency selective case.

IV. INPUT-OUTPUT COUPLING STRATEGIES

The capacity analysis presented in Section III is important, but it only serves as an upper limit on the achievable rate. This limit can only be achieved by making use of all available spatial modes. In theory, one can always design a fiber with a sufficiently small core radius such that a desired number of modes propagate through the fiber [6]. In reality, one has to rely on currently installed optical fibers and available technologies. The state-of-the-art OM3 and OM4 MMF technologies have core radii of $50 \mu\text{m}$ with hundreds of propagation modes. Unfortunately, having a 100×100 MIMO system is neither physically nor computationally realizable at the moment. This means that a more careful look at the effective channel capacity has to be considered. This is why we now focus on the case when N_t transmit laser sources and N_r receivers are used. For most of this section, we assume that intermodal and chromatic dispersions are negligible. Even though this may seem like a restriction, this assumption serves to simplify the discussion and presentation of input-output coupling strategies. The results and procedures we present offer insight and can be extended to the more general frequency selective case.

A. Input-Output Coupling Model

The input coupling is described by \mathbf{C}_I , an $M \times N_t$ matrix, and the output coupling is described by \mathbf{C}_O , an $N_r \times M$ matrix. Here, M is much larger than N_t and N_r and the overall response is given by

$$\begin{aligned} \mathbf{H}_t &= \mathbf{C}_O \mathbf{H}^{(K)} \dots \mathbf{H}^{(1)} \mathbf{C}_I \\ &= \mathbf{C}_O \mathbf{H} \mathbf{C}_I \end{aligned} \quad (33)$$

Therefore, for a single instantiation of \mathbf{H}_t , the capacity of the channel is given by

$$C(\mathbf{H}_t) = \log \det \left(\mathbf{I}_{N_t} + \frac{\text{SNR}}{N_t} \mathbf{H}_t \mathbf{H}_t^* \right) \quad (34)$$

The input-output coupling coefficients (entries of \mathbf{C}_I and \mathbf{C}_O) are complex quantities capturing the effect of both power and phase coupling into and out of the fiber. These coefficients are determined by the system geometry and launch conditions. For example, in order to study the input coupling profile of each light source one needs to specify its exact geometry and launching angle, and then solve the overlap integrals: two dimensional inner products between the laser's spatial patterns and those of each mode

$$c_{ij} = \int \int \phi_i(x, y) \phi_{s_j}(x, y) dx dy \quad (35)$$

where c_{ij} is the $(i, j)^{th}$ entry of \mathbf{C}_I , $\phi_i(x, y)$ is the i^{th} mode spatial pattern, and $\phi_{s_j}(x, y)$ is the j^{th} laser source spatial pattern. However, this procedure is cumbersome and offers little insight on the underlying channel physics. In what follows, we provide a simple condition on the input-output couplers. This condition will prove useful when we present an input-output scheme that maximizes the achievable rate of the overall system (Section IV-B) and impose a statistical model for \mathbf{C}_I and \mathbf{C}_O (Section IV-C).

Theorem 4.1: If we neglect the power lost due to input coupling inefficiencies, then a necessary and sufficient condition for \mathbf{C}_I to be an input coupling matrix is given by

$$(\mathbf{c}_i, \mathbf{c}_j) = \delta_{ij} \quad (36)$$

where \mathbf{c}_i represents the i^{th} column of \mathbf{C}_I and (\mathbf{a}, \mathbf{b}) denotes the standard Euclidean inner product between the vectors \mathbf{a} and \mathbf{b} . This means that the columns of \mathbf{C}_I should form a complete orthonormal basis for \mathbb{C}^{N_t} . Similarly, if we neglect the power lost due to output coupling inefficiencies, then the rows of \mathbf{C}_O should form a complete orthonormal basis for \mathbb{C}^{N_r} .

Proof: Satisfying the energy conservation principle requires that

$$\|\mathbf{C}_I \mathbf{x}\|^2 = \|\mathbf{x}\|^2 \quad \forall \mathbf{x} \in \mathbb{C}^{N_t} \quad (37)$$

This means that the energy of the input vector should be equal to the energy of the mode vector at the input of the fiber. This condition holds whenever the mapping \mathbf{C}_I is a linear isometry mapping. In the special case where \mathbf{C}_I is a square matrix, a classical result in linear algebra states that \mathbf{C}_I has to be a unitary matrix [24]. However, \mathbf{C}_I is a tall $M \times N_t$ ($M \gg N_t$) rectangular matrix. In this case, the condition in (37) can be rewritten as

$$(\mathbf{C}_I \mathbf{x}, \mathbf{C}_I \mathbf{x}) = (\mathbf{x}, \mathbf{x}) \quad \forall \mathbf{x} \in \mathbb{C}^{N_t} \quad (38)$$

or equivalently as

$$(\mathbf{x}, [\mathbf{C}_I^* \mathbf{C}_I - \mathbf{I}_{N_t}] \mathbf{x}) = 0 \quad \forall \mathbf{x} \in \mathbb{C}^{N_t} \quad (39)$$

If $\mathbf{C}_I^* \mathbf{C}_I = \mathbf{I}_{N_t}$, the condition in (39) holds and \mathbf{C}_I preserves the norm. This choice ensures that the columns of \mathbf{C}_I form a complete orthonormal basis for \mathbb{C}^{N_t} . However, this only proves the sufficiency part of the theorem. To prove the necessity part, we consider $\mathbf{B} = \mathbf{C}_I^* \mathbf{C}_I - \mathbf{I}_{N_t}$ and show that if (39) holds, then it is equal to zero. It can be easily verified that if \mathbf{B} is a diagonal matrix, then $(\mathbf{x}, \mathbf{B}\mathbf{x}) = 0 \quad \forall \mathbf{x} \in \mathbb{C}^{N_t}$ implies that $\mathbf{B} = \mathbf{0}$. The same observation holds if \mathbf{B} is diagonalizable. In this case, one can choose an orthonormal basis of eigenvectors and map $(\mathbf{x}, \mathbf{B}\mathbf{x}) = 0 \quad \forall \mathbf{x} \in \mathbb{C}^{N_t}$ to $(\tilde{\mathbf{x}}, \mathbf{D}\tilde{\mathbf{x}}) = 0 \quad \forall \tilde{\mathbf{x}} \in \mathbb{C}^{N_t}$ where \mathbf{D} is a diagonal matrix. In our case, \mathbf{B} is Hermitian and hence it is unitarily diagonalizable so that $\mathbf{B} = \mathbf{0}$ or alternatively, $\mathbf{C}_I^* \mathbf{C}_I = \mathbf{I}_{N_t}$ as desired. A similar proof can be carried out to show that $\mathbf{C}_O \mathbf{C}_O^* = \mathbf{I}_{N_r}$. ■

We note that even though $\mathbf{C}_I^* \mathbf{C}_I = \mathbf{I}_{N_t}$, $\mathbf{C}_I \mathbf{C}_I^* \neq \mathbf{I}_{N_t}$ because \mathbf{C}_I is of full column rank, but not of full row rank. We now use this property to show that \mathbf{C}_I and \mathbf{C}_O should have a special structure.

Theorem 4.2: The input-output coupling matrices \mathbf{C}_I and \mathbf{C}_O can be expressed as

$$\mathbf{C}_I = \mathbf{U}_I \begin{bmatrix} \mathbf{I}_{N_t} \\ \mathbf{0}_{(M-N_t) \times N_t} \end{bmatrix} \mathbf{V}_I^* \quad (40)$$

$$\mathbf{C}_O = \mathbf{U}_O [\mathbf{I}_{N_r} \mathbf{0}_{N_r \times (M-N_r)}] \mathbf{V}_O^* \quad (41)$$

where \mathbf{U}_I and \mathbf{V}_O^* are $M \times M$ unitary matrices, \mathbf{V}_I^* is an $N_t \times N_t$ unitary matrix, and \mathbf{U}_O is an $N_r \times N_r$ unitary matrix.

Proof: By the singular value decomposition (SVD), $\mathbf{C}_I = \mathbf{U}_I \mathbf{\Lambda}_I \mathbf{V}_I^*$ and $\mathbf{C}_O = \mathbf{U}_O \mathbf{\Lambda}_O \mathbf{V}_O^*$ [24]. The non-zero singular values of \mathbf{C}_I are the square roots of the eigenvalues of $\mathbf{C}_I^* \mathbf{C}_I$, and $\mathbf{C}_I^* \mathbf{C}_I = \mathbf{I}_{N_t}$. A similar argument holds for \mathbf{C}_O . ■

B. Input-Output Coupling Strategies

In this section, we assume that $N_t = N_r$. When CSI is available at the transmitter and the design of \mathbf{C}_I and \mathbf{C}_O is affordable, a desirable choice for the input-output couplers is the one that maximizes the system's capacity

$$\begin{aligned} (\mathbf{C}_I^{\text{opt}}, \mathbf{C}_O^{\text{opt}}) &= \arg \max_{(\mathbf{C}_I, \mathbf{C}_O)} \log \det \left(\mathbf{I}_{N_r} + \frac{\text{SNR}}{N_t} \mathbf{H}_t \mathbf{H}_t^* \right) \\ &= \arg \max_{(\mathbf{C}_I, \mathbf{C}_O)} \sum_{n=1}^N \log \left(1 + \frac{\text{SNR}}{N_t} \lambda_n^2 \right) \end{aligned} \quad (42)$$

where the λ_n^2 's are the eigenvalues of $\mathbf{H}_t \mathbf{H}_t^*$. We note that $\mathbf{C}_I^{\text{opt}}$ and $\mathbf{C}_O^{\text{opt}}$ should have a structure compliant with (40) and (41), respectively. Instead of solving the above constrained optimization problem, we provide an intuitive choice for $(\mathbf{C}_I, \mathbf{C}_O)$ and argue that it leads to a maximized overall capacity through simulations.

Proposition 4.1: The capacity of the overall system in (34) is independent of the choice of \mathbf{V}_I^* and \mathbf{U}_O from (40) and (41).

Proof: The capacity of the overall system is given by

$$\begin{aligned}
C(\mathbf{H}_t) &= \log \det \left(\mathbf{I}_{N_t} + \frac{\text{SNR}}{N_t} \mathbf{H}_t \mathbf{H}_t^* \right) \\
&= \log \det \left(\mathbf{I}_{N_t} + \frac{\text{SNR}}{N_t} \mathbf{C}_O \mathbf{H} \mathbf{C}_I \mathbf{C}_I^* \mathbf{H}^* \mathbf{C}_O^* \right) \\
&= \log \det \left(\mathbf{I}_{N_t} + \frac{\text{SNR}}{N_t} \mathbf{U}_O \Lambda_O \mathbf{V}_O^* \mathbf{H} \mathbf{U}_I \Lambda_I \Lambda_I^* \mathbf{U}_I^* \mathbf{H}^* \mathbf{V}_O \Lambda_O^* \mathbf{U}_O^* \right) \\
&= \log \det \left(\mathbf{I}_{N_t} + \frac{\text{SNR}}{N_t} \Lambda_O \mathbf{V}_O^* \mathbf{H} \mathbf{U}_I \Lambda_I \Lambda_I^* \mathbf{U}_I^* \mathbf{H}^* \mathbf{V}_O \Lambda_O^* \right) \tag{43}
\end{aligned}$$

Therefore, the capacity of the overall system is independent of \mathbf{V}_I^* and \mathbf{U}_O and hence, without loss of generality, we will assume that they are both equal to the identity matrix. ■

The following input-output coupling scheme is suggested

$$\mathbf{C}_I = \mathbf{V}_H \begin{bmatrix} \mathbf{I}_{N_t} \\ \mathbf{0}_{(M-N_t) \times N_t} \end{bmatrix} \tag{44}$$

$$\mathbf{C}_O = [\mathbf{I}_{N_r} \mathbf{0}_{(M-N_t) \times N_t}] \mathbf{U}_H^* \tag{45}$$

where \mathbf{V}_H and \mathbf{U}_H have been defined in (19). Choosing $\mathbf{V}_O = \mathbf{U}_H$, $\mathbf{U}_O = \mathbf{I}_{N_t}$, $\mathbf{U}_I = \mathbf{V}_H$, and $\mathbf{V}_I = \mathbf{I}_{N_t}$ leads to an overall response given by

$$\begin{aligned}
\mathbf{H}_t &= [\mathbf{I}_N \mathbf{0}_{(M-N) \times N}] \Lambda_H \begin{bmatrix} \mathbf{I}_N \\ \mathbf{0}_{(M-N) \times N} \end{bmatrix} \\
&= \text{diag}(\lambda_1, \dots, \lambda_N)
\end{aligned} \tag{46}$$

Thus, the overall MIMO channel is transformed into a set of parallel AWGN channels. Moreover, since the SVD in (19) sorts the singular values in decreasing order, the signal energy has been restricted to the N_t (out of M) least lossy end-to-end eigenmodes. The capacity achieved by this choice of input-output coupling is

$$C(\mathbf{H}_t) = \sum_{n=1}^{N_t} \log \left(1 + \frac{\text{SNR}}{N_t} e^{\rho_n} \right) \quad \text{b/s/Hz} \tag{47}$$

This capacity could be further increased by pre-processing \mathbf{x} via a diagonal power allocation matrix \mathbf{K} using waterfilling. Our strategy is intuitive since we only have N_t degrees of freedom so it would be wise if we use the N_t least lossy end-to-end eigenmodes to transmit. We note that even though the effective end-to-end fiber response shows that we have used the N_t best end-to-end eigenmodes only, N_t signals were coupled to and collected from all the available physical modes at the input and output of the fiber. Nonetheless, achieving (47) requires, as discussed before, having CSI at transmitter and using adaptive spatial filters which is typically hard to implement. Even though we did not prove that the above strategy is capacity optimal, our simulations section will show that it appears to maximize the capacity of the overall system.

C. Random Input-Output Coupling

The design of reconfigurable input-output couplers is expensive and assumes the availability of CSI at the transmitter (which is only feasible when the channel is varying slowly). More importantly, in many cases, the coupling coefficients are affected by continuous vibrations and system disturbances. Thus, full control over \mathbf{C}_I and \mathbf{C}_O is not always affordable. In this section, we analyze the capacity when the user does not have control over \mathbf{C}_I and \mathbf{C}_O . This will give us better insight on the achievable capacity of MIMO MMF systems. We model the coupling coefficients as time varying random variables and impose a physically inspired distribution that respects both the fundamental energy preservation constraint and the maximum entropy principle. Even though we focus on describing the statistical model of \mathbf{C}_I , our discussion applies equally well for \mathbf{C}_O .

For an $M \times M$ square matrix \mathbf{A} , the energy conservation principle confirms that \mathbf{A} should belong to $\mathbb{U}(M)$. It was proven in [15] that since a Haar measure exists over $\mathbb{U}(M)$, one could define a uniform distribution over $\mathbb{U}(M)$. Therefore, we choose a random setting where the input coupling matrix \mathbf{C}_I has its N_t columns randomly selected from a square matrix \mathbf{A} that is uniformly distributed over $\mathbb{U}(M)$. This distribution ensures that the columns of \mathbf{C}_I form a complete orthonormal basis for \mathbb{C}^{N_t} and gives equal probability measure for all such possible vectors. In other words, \mathbf{C}_I is uniformly distributed over a Stiefel manifold $\mathbb{V}_{N_t}(\mathbb{C}^M)$. Appendix A shows how we can generate \mathbf{C}_I and \mathbf{C}_O from an $M \times M$ matrix with i.i.d. Gaussian entries. The ergodic capacity of the overall system can now be computed by averaging over the statistics of the input-output couplers and the statistics of the fiber response. Similarly, one could also compute the probability of an outage event by obtaining the cumulative distribution function (CDF) of the capacity, which now depends on the statistics of \mathbf{C}_I and \mathbf{C}_O .

D. Discussion

We have evaluated the capacity of both controlled and uncontrolled MIMO MMF systems. As discussed in Section IV-B, the controlled case refers to the case when CSI is available at the transmitter side and there is full control over the input-output couplers. The uncontrolled case refers to the random coupling model presented in Section IV-C. In our simulations, we numerically computed the ergodic capacity using (24), with \mathbf{H} replaced by $\mathbf{H}_t = \mathbf{C}_O \mathbf{H} \mathbf{C}_I$. The average in (24) is taken over the statistics of the channel and the input-output couplers for the uncontrolled case. For reference, we included plots of the capacity when

- all mode dependent losses are equal to zero and there is no mode coupling ($K = 1$ and $\xi = 0$); hence the channel has unity eigenmodes. A fiber with such properties will be referred to as an *ideal fiber*.
- the fiber core radius is chosen so that only N_t modes can propagate. In this case the input and output coupling matrices are unitary matrices.

In this analysis, we consider $N_t = N_r = 4$, $K = 256$, $\xi = 4$ dB, and $M = 100$. Comparing Figures 4 and 3b, we observe that the capacity of a 4×4 system over a 100-mode fiber is inferior to the intrinsic capacity of the fiber (i.e., when all the modes are used). This result is expected since we are using 4 out of 100 available degrees of freedom. At moderate SNR values the loss in capacity is about 6 dB. On the other hand, observe, from Figure

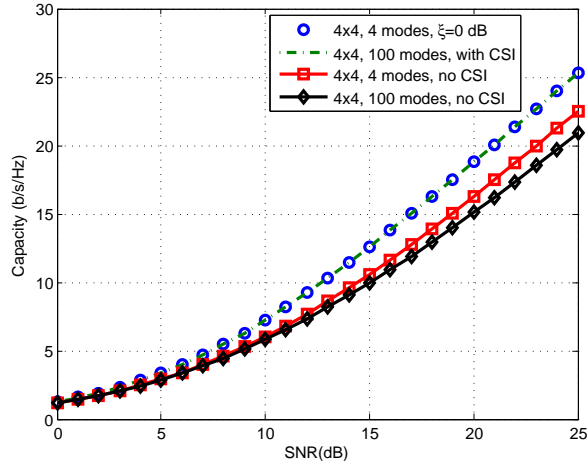


Fig. 4: Achievable capacity of a 4×4 MIMO MMF system

4, that the performance of an uncontrolled 4×4 system over a 100-mode fiber is close to that of a system with 4 modes. Thus, currently installed fibers could be used without significant loss in capacity. We also note that, by using the input-output coupling strategy presented in Section IV-B, performance equal to that of an ideal fiber can be achieved. This is explained by revisiting Figure 2 which shows the probability distribution of the end-to-end MDL values when $M = 100$. We observe that in this case we only use the best 4 eigenmodes to transmit the signal. As such, it is highly probable that these 4 (out of 100) modes will have close to zero end-to-end mode-dependent losses, and thus the performance is almost equal to that of an ideal fiber (even when ξ is large). The larger M is, the closer the capacity of a controlled fiber can get to that of an ideal fiber. Finally, one could argue that coupling a reasonable number of inputs to a fiber with hundreds of modes is advantageous since the fiber's peak power constraint is proportional to the number of modes (recall that more propagation modes means larger core radius). This means that compared to an N_t -mode fiber, a higher capacity could be achieved if we signal over an $M \gg N_t$ -mode fiber since the total power budget can now be increased.

V. CONCLUSION

MIMO communications over optical fibers is an attractive solution to the ever increasing demand for Internet bandwidth. We presented a propagation model that takes input-output coupling into account for MIMO MMF systems. A coupling strategy was suggested and simulations showed that the capacity of an $N_t \times N_t$ MIMO system over a fiber with $M \gg N_t$ modes can approach the capacity of an ideal fiber with N_t modes. A random input-output coupling model was used to describe the behavior of the system when the design of the input-output couplers is not available. The results illustrated that, under random coupling, the capacity of an $N_t \times N_t$ MIMO system over a fiber with $M \gg N_t$ modes is almost equal to that of an N_t -mode fiber.

APPENDIX

Our method for generating random unitary matrices is based on the QR decomposition procedure [15]. In this case, \mathbf{A} is constructed as follows:

- 1) Generate an $M \times M$ matrix \mathbf{Z} with i.i.d. complex Gaussian entries.
- 2) Obtain the QR decomposition of \mathbf{Z} ; $\mathbf{Z} = \mathbf{Q}\mathbf{R}$.
- 3) Form the following diagonal matrix:

$$\mathbf{\Lambda} = \begin{pmatrix} \frac{r_{11}}{|r_{11}|} & & & & \\ & \frac{r_{22}}{|r_{22}|} & & & \\ & & \ddots & & \\ & & & \ddots & \\ & & & & \frac{r_{MM}}{|r_{MM}|} \end{pmatrix} \quad (48)$$

where $\{r_{ii}\}_{i=1}^M$ are the diagonal entries of \mathbf{R} .

- 4) Let $\mathbf{A} = \mathbf{\Lambda}\mathbf{Q}$.

In the above construction, \mathbf{A} is obviously unitary since \mathbf{Q} is unitary. Furthermore, it can be shown that \mathbf{A} has a uniform distribution over $\mathbb{U}(M)$. To generate the input coupling matrix, the following method is used:

- 1) Generate an $M \times M$ unitary matrix \mathbf{A} (as described above).
- 2) Choose N_t columns randomly from \mathbf{A} to form \mathbf{C}_I .

A similar approach can be taken to generate \mathbf{C}_O . In this case, N_r columns are selected randomly from \mathbf{A} to represent the rows of \mathbf{C}_O .

REFERENCES

- [1] R. W. Tkach, "Scaling optical communications for the next decade and beyond," *Bell Labs Technical Journal*, vol. 14, no. 4, pp. 3–9, 2010.
- [2] P. Winzer, "Modulation and multiplexing in optical communications," in *Lasers and Electro-Optics, 2009 and 2009 Conference on Quantum electronics and Laser Science Conference. CLEO/QELS 2009. Conference on*, June 2009, pp. 1–2.
- [3] P. J. Winzer and G. J. Foschini, "MIMO capacities and outage probabilities in spatially multiplexed optical transport systems," *Opt. Express*, vol. 19, pp. 16 680–16 696, 2011.
- [4] A. F. Benner, M. Ignatowski, J. A. Kash, D. M. Kuchta, and M. B. Ritter, "Exploitation of optical interconnects in future server architectures," *IBM Journal of Research and Development*, vol. 49, no. 4.5, pp. 755–775, July 2005.
- [5] Y. Koike and S. Takahashi, "Plastic optical fibers: Technologies and communication links," in *Optical Fiber Telecommunications V A*, I. P. Kaminow, T. Li, and A. E. Willner, Eds. Burlington: Academic Press, 2008, pp. 593–603.
- [6] G. P. Agarwal, *Fiber-Optic Communication Systems*, 3rd ed. Wiley, 2002.
- [7] C. Shannon and W. Weaver, *The Mathematical Theory of Communication*. University of Illinois Press, Urbana, 1949.
- [8] E. Telatar, "Capacity of multi-antenna Gaussian channels," *European Transactions on Telecommunications*, vol. 10, no. 6, pp. 585–595, 1999.
- [9] G. Foschini and M. Gans, "On limits of wireless communications in a fading environment when using multiple antennas," *Wireless Personal Communications*, vol. 6, pp. 311–335, 1998, 10.1023/A:1008889222784. [Online]. Available: <http://dx.doi.org/10.1023/A:1008889222784>
- [10] D. Tse and P. Viswanath, *Fundamentals of Wireless Communication*. Cambridge University Press, 2005.
- [11] H. R. Stuart, "Dispersive multiplexing in multimode optical fiber," *Science*, vol. 289, no. 5477, pp. 281–283, 2000. [Online]. Available: <http://www.sciencemag.org/content/289/5477/281.abstract>

- [12] A. Shah, R. Hsu, A. Tarighat, A. Sayed, and B. Jalali, "Coherent optical MIMO (COMIMO)," *Lightwave Technology, Journal of*, vol. 23, no. 8, pp. 2410 – 2419, Aug. 2005.
- [13] K.-P. Ho and J. M. Kahn, "Mode-dependent loss and gain: statistics and effect on mode-division multiplexing," *Opt. Express*, vol. 19, pp. 16 612–16 635, 2011.
- [14] K.-P. Ho and J. Kahn, "Frequency diversity in mode-division multiplexing systems," *Lightwave Technology, Journal of*, vol. 29, no. 24, pp. 3719 –3726, Dec. 15, 2011.
- [15] F. Mezzadri, "How to generate random matrices from the classical compact groups," *arXiv preprint math-ph/0609050*, 2006.
- [16] D. Petz and J. Réffy, "On asymptotics of large haar distributed unitary matrices," *Periodica Mathematica Hungarica*, vol. 49, no. 1, pp. 103–117, 2004.
- [17] G. C. Papan and R. E. Blahut, "Lightwave Communication Systems," unpublished draft, 2012.
- [18] R. Khosravani, I. T. Lima Jr., P. Ebrahimi, E. Ibragimov, A. Willner, and C. Menyuk, "Time and frequency domain characteristics of polarization-mode dispersion emulators," *Photonics Technology Letters, IEEE*, vol. 13, no. 2, pp. 127 –129, Feb. 2001.
- [19] K.-P. Ho and J. Kahn, "Statistics of group delays in multimode fiber with strong mode coupling," *Lightwave Technology, Journal of*, vol. 29, no. 21, pp. 3119 –3128, Nov. 1, 2011.
- [20] T. M. Cover and J. A. Thomas, *Elements of Information Theory*. Wiley-Interscience, 2006.
- [21] E. Alon, V. Stojanovic, J. Kahn, S. Boyd, and M. Horowitz, "Equalization of modal dispersion in multimode fiber using spatial light modulators," in *Global Telecommunications Conference, 2004. GLOBECOM '04. IEEE*, Nov.-3 Dec. 2004, pp. 1023 – 1029.
- [22] H. Chen, H. van den Boom, and A. Koonen, "30gbit/s 3×3 optical mode group division multiplexing system with mode-selective spatial filtering," in *Optical Fiber Communication Conference and Exposition (OFC/NFOEC), 2011 and the National Fiber Optic Engineers Conference*, March 2011, pp. 1 –3.
- [23] W. Shieh, H. Bao, and Y. Tang, "Coherent optical OFDM: theory and design," *Opt. Express*, vol. 16, no. 2, pp. 841–859, Jan 2008. [Online]. Available: <http://www.opticsexpress.org/abstract.cfm?URI=oe-16-2-841>
- [24] G. Shilov, *Linear Algebra*. Prentice-Hall Inc, 1971.